Int. J. Heat Mass Transfer. Vol. 22, pp. 749–761
Pergamon Press Ltd. 1979. Printed in Great Britain

MELTING OF POWDER GRAINS IN A PLASMA FLAME

JERZY K. FISZDON*
Institute of Nuclear Research, Department of Plasma Physics and Technology,
05-400, Otwock, Poland

(*Received* 11 *May* 1976 *and in revised form* 7 *July* 1978)

Abstract—A numerical method to determine the heat transfer and phase change processes of a spherical particle in a jet stream is deduced. The variations of the thermophysical properties of the particle and of the plasma with temperature are taken into account. An example of alumina particles heated in an argon–hydrogen plasma jet is given. The numerical results, compared with experimental measurements of surface temperature, particle velocity and diameter show good agreement.

NOMENCLATURE

c, mixture concentration;
c_p, specific heat;
C_D, drag coefficient;
D, particle diameter;
D_{ab}, molecular diffusion coefficient;
L, latent heat of phase change;
q, heat flux;
r, radius;
t, time;
T, temperature;
V, v, velocity;
Nu, Nusselt number;
Pr, Prandtl number;
Re, Reynolds number;
Sc, Schmidt number;
Sh, Sherwood number.

Greek symbols

α, heat transfer coefficient;
β, mass transfer coefficient;
ε, material emittance;
λ, heat conductivity;
η, viscosity;
ρ, density.

Subscripts

Quantities without subscripts refer to particle
g, gas;
B, boundary;
f, fusion;
e, evaporation;
k, solidification.

1. INTRODUCTION

IN THE use of plasma torches for spraying, the intensive heat transfer between the gaseous medium and the solid or liquid particles contained in it is an important problem. A numerical method for calculating the motion and heating including phase changes for spherical particles during their movement in the hot gas jet with known parameters is presented. The variation of the flow parameters in the jet and the thermophysical properties of the gas and the particles with temperature was taken into consideration.

Results of calculations made for Al_2O_3 particles are compared with experimental data.

This problem can be divided in two parts: heat transfer between the particle and the gas medium and heat conduction and phase changes inside the particle.

The heat-transfer problem inside a spherical particle has an analytical solution for the case of constant material parameters only or for some special cases of variation of material properties with the radius [1, 2]. The heat-transfer problem with phase change has some analytical solutions for special simplified cases [3, 4]. Heat transfer between the gaseous medium and spherical particles was thoroughly examined in the case of "cold" gas. The authors of [5, 6] give the following relation for Nusselt number:

$$Nu = 2 + bRe^m Pr^n. \tag{1}$$

In some papers [7, 8] related to dissociated gases and high temperature differences, the use of the correction factor $f(T) = (\rho_\infty \eta_\infty / \rho_s \eta_s)^p$ is recommended. This takes into account the change of gas parameters inside the boundary layer (the index ∞ refers to the gas temperature and s to the temperature of the particle surface). In the present paper for the calculations of the heat transfer between the gas and the particle, equation (1) given in [5] was used.

The parameters of the plasma torch type PN-110 used for the numerical calculations are given below:

voltage—52 V; argon flow—2.6 Nm^3/h;
current—500 A; hydrogen flow—0.4 Nm^3/h;
efficiency—48%.

*Presently at: Warsaw Technical University, Institute of Heat Engineering, Nowowiejska 25, 00-665 Warsaw, Poland.

2. PARTICLE MOTION

The particle motion, disregarding the negligible influence of mass variation on the impulse change, according to [17] is:

$$\frac{d\bar{v}}{dt} = 0.75\frac{\rho_g}{\rho D}(\bar{V}_g - \bar{v})^2 C_D. \tag{2}$$

The drag coefficient C_D according to [9] depending on the Reynolds number range is:

$$\begin{aligned} C_D &= 24Re^{-1}, && \text{for } Re < 2; \\ C_D &= 18.5Re^{-0.6}, && \text{for } 2 < Re < 500; \\ C_D &= 0.44, && \text{for } Re > 500. \end{aligned} \tag{3}$$

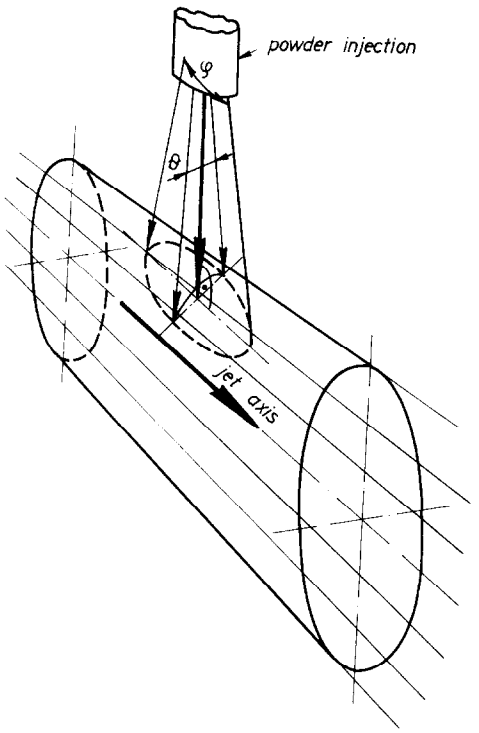

FIG. 1. Model of powder injection.

In our case it is convenient to use (2) in the following form:

$$\bar{v}\frac{d\bar{v}}{dx} = 0.75\frac{\rho_g}{\rho \cdot D}C_D(\bar{V}_g - \bar{v})^2. \tag{4}$$

In the case when the gas velocity is varying and the gas and particle properties depend on the temperature, i.e. vary with their position, (4) is an Abel type equation and then no analytical solution exists.

In the case of plasmatrones, where the gas velocity and the powder injection velocity (Fig. 1) are not parallel, equation (4) written in the two-dimensional system is used. The solution of this system can be obtained numerically.

3. HEAT TRANSFER BETWEEN THE GAS AND THE PARTICLE SURFACE

From Newton's law, the heat flux to the particle is

$$q = \alpha \cdot \Delta T, \tag{5}$$

where ΔT is the temperature difference between gas and particle surface and α is the heat-transfer coefficient, which includes the heat transfer by convection (α_p), radiation (α_r) and mass convection (β).

The heat-transfer coefficient due to the heat convection was taken from [10] with a correction coefficient from [11] in the form:

$$Nu = \frac{\alpha_p D}{\lambda_g} = (2 + 0.6Re^{1/2}Pr^{1/3})\left(\frac{\rho_\infty \eta_\infty}{\rho_s \eta_s}\right)^{0.6}. \tag{6}$$

Radiation from the particle (which is only about 5% of the total exchanged heat [12]) was taken into account by:

$$\alpha_r = -\sigma\varepsilon T_s^4/\Delta T, \tag{7}$$

where T_s is the particle surface temperature and the black body radiation constant is $\sigma = 5.7\,\mathrm{Wm}^{-2}\,\mathrm{deg}^{-4}$. In (7) the heat losses to a low temperature surrounding were assumed.

The mass convection coefficient β [13] can be taken from

$$Sh = \frac{\beta D}{D_{ab}C} = 2 + 0.6Re^{1/2}Sc^{1/3}. \tag{8}$$

These coefficients are variable depending on the local variation of the thermodynamic and flow parameters.

4. HEAT CONDUCTION INSIDE THE PARTICLE

4.1. *Heat-transfer equation*

For non-stationary flow over a body with temperature dependent properties without external sources of heat, the heat conduction is described by the following differential equation

$$\rho(T)c_p(T)\frac{\partial T}{\partial t} = \nabla[\lambda(T)\nabla T]. \tag{9}$$

In the case of small particles the usual assumption of spherical symmetry [14] is made, which leads to the existence of spherical isothermal surfaces. An additional justification for this assumption is the probable rotation of the particles due to asymmetrical injection of the particles into the jet. In this case equation (9) written in spherical coordinates becomes

$$\rho(T)c_p(T)\frac{\partial T}{\partial t} = r^{-2}\frac{\partial}{\partial r}\left[\lambda(T)r^2\frac{\partial T}{\partial r}\right], \tag{10}$$

where r is the distance from the center of the sphere.

The initial temperature distribution is

$$T(r, 0) = f(r) \tag{11}$$

and the symmetry condition can be written as

$$\left.\frac{\partial T}{\partial r}\right|_{r=0} = 0. \tag{12}$$

The remaining boundary conditions for the particle depend on its state and will be given below for the different cases considered.

4.2. *The case of a sphere in a one-phase state*

In this case for time $t > 0$ and radius $0 < r < D/2$ equation (10) with condition (12) holds. The condition at the outer boundary follows from the heat balance (5) and is given by:

$$\lambda(T)\frac{\partial T}{\partial r}\bigg|_{r=D/2} = (\alpha_r+\alpha_p)(T_g-T)\bigg|_{r=D/2}. \quad (13)$$

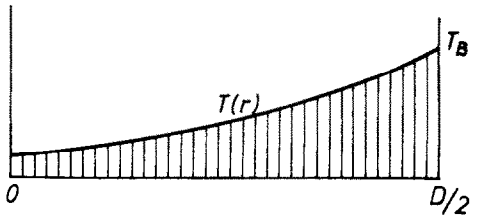

4.3. *The case of two-phase sphere*

When the particle surface reaches the melting temperature, a phase change process will begin. The particle consists then of two layers: inner—solid and outer—liquid, and a phase boundary r_f moves inside the particle. A part of the heat delivered from the gas will be used in the melting process. For the internal

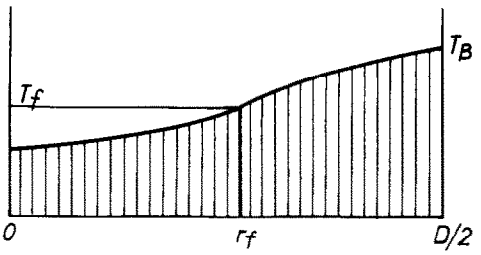

region of the sphere $0 < r < r_f(t)$ the boundary conditions for equation (10) are given by (12) at $r = 0$ and the following conditions at $r = r_f(t)$:

$$\lambda(T)\frac{\partial T}{\partial r}\bigg|_{r=r_f-0} = \lambda(T)\frac{\partial T}{\partial r}\bigg|_{r=r_f+0} + L_f\rho(T_f)\frac{dr_f}{dt} \quad (14)$$

and

$$T\big|_{r_f-0} = T\big|_{r_f+0} = T_f. \quad (15)$$

For the external region, i.e. $r_f(t) < r < D/2$, the inner boundary conditions for equation (10) at $r = r_f(t)$ are given also by (14) and (15) and the outer boundary condition at $r = D/2$ is given by (13).

Similarly in the case of the solidification of a liquid sphere the same relations hold, the only difference being that the outer layer is now solid and the inner liquid. At the interface of the two phases heat is now emitted and not absorbed as in the previous case.

4.4. *The case of intense evaporation*

The difference between this case and the one described above consists in the appearance of a moving outer sphere boundary, r_e, due to evaporation of the outer layer of the particle. The heat transferred from the gas is now used partially for evaporation, hence the boundary condition (13) will be modified by addition of a term taking into

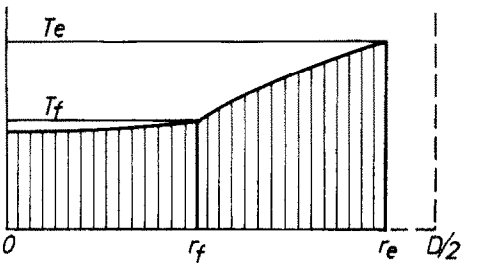

account the heat of evaporation:

$$\lambda(T)\frac{\partial T}{\partial r}\bigg|_{r=r_e} = (\alpha_r+\alpha_p)(T_g-T)\bigg|_{r=r_e} + L_e\rho\frac{dr_e}{dt} \quad (16)$$

and in the case of intensive evaporation, the surface temperature will be equal to the boiling temperature:

$$T(r_e, t) = T_e. \quad (17)$$

In this case equation (10) is valid with boundary conditions (12) at the centre, (14) and (15) at the solid–liquid interface and (16) and (17) at the outer boundary.

In the case of a single-phase particle with evaporation at the surface, the boundary conditions for equation (10) are (12) at the centre and (16),(17) at the outer surface.

The above relations were used only in the cases where the temperature of the particle surface reached the temperature of evaporation. When it was lower the conditions described in 4.6. (with temperature dependent heat of evaporation) are relevant.

4.5. *The case of solidification*

This case occurs when the temperature of the surrounding medium and the temperature of the particle surface drops below the temperature of solidification:

$$T_g < T_f > T_B, \quad (18)$$

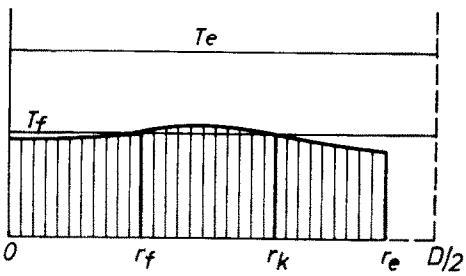

whereas the outer layer of the particle was liquid. At the boundary of solidification r_k heat will be emitted. The conditions at this boundary will be analogous to those described in 4.3.:

$$\lambda(T)\left.\frac{\partial T}{\partial r}\right|_{r_k-0} = \lambda(T)\left.\frac{\partial T}{\partial r}\right|_{r_k+0} + L_f\rho(T_f)\frac{dr_k}{dt}, \tag{19}$$

with:

$$T(r_k) = T_f. \tag{20}$$

The boundary conditions for (10) are then (12)–(15), (19), (20).

4.6. *The case of diffusion of the vaporized particle material*

The diffusion of the vaporized particle material into the gas can be described as follows:

vaporized mass flux:

$$\frac{dm}{dt} = -4\pi r_e^2\rho\frac{dr_e}{dt}; \tag{21}$$

from Stefan's law [13]:

$$\frac{dm}{dt} = 4\pi r_e^2 M\beta\ln\frac{p_0-p_f}{p_0-p(T)}, \tag{22}$$

where p_0, p_f, $p(T)$ are partial pressures respectively to saturation, melting temperature and a temperature T, M is the molecular weight.

Substituting (21) into (22):

$$\frac{dr_e}{dt} = -M\beta\ln\frac{p_0-p_f}{p_0-p(T)}. \tag{23}$$

In this case boundary condition (13) with (23) become:

$$\lambda(T)\left.\frac{\partial T}{\partial r}\right|_{r_e} = (\alpha_r+\alpha_p)(T_g-T)\Big|_{r_e} - L_e(T)M\beta\ln\frac{p_0-p_f}{p_0-p(T)}. \tag{24}$$

5. NUMERICAL METHOD OF SOLUTION

As was shown in [15] the non-stationary heat-transfer problem with a phase change has a unique solution. To solve this problem in the general case a closed finite difference scheme was used. This procedure insures the stability of the solution for any grid. The time differential in the i-node of the mesh is approximated by the backward difference operator:

$$\left(\frac{\partial T}{\partial t}\right)_i \approx (T_i - T_i^-)/\Delta t \tag{25}$$

and the space differentials are approximated by central difference operators in the inner net mesh:

$$\left(\frac{\partial T}{\partial r}\right)_i \approx (T_{i+1/2} - T_{i-1/2})/\Delta r \tag{26}$$

or by forward difference operators at the boundary:

$$\left(\frac{\partial T}{\partial r}\right)_i \approx (T_{i+1} - T_i)/\Delta r. \tag{27}$$

T_i is the actual temperature at the radius r_i and T_i^- the temperature at the radius r_i in the previous time step differing by Δt from the present step, Δt is time difference and Δr the space difference.

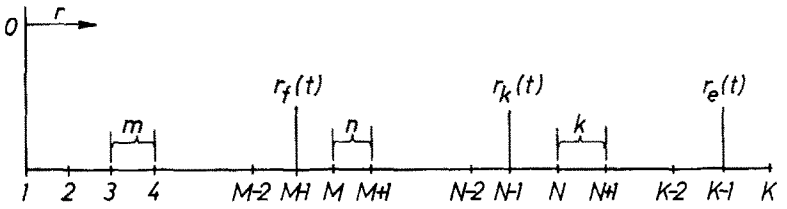

In the fully developed case [according to (4.5)], the sphere radius can be divided as follows:
—the centre of the sphere ($r = 0$) is at point $i = 1$, melting radius (r_f) at point $i = M-1$, evaporation or external radius (r_e) at point $i = K-1$ and solidification radius (r_k) at point $i = N-1$. The point K is outside the sphere boundary—in gas. The internal solid layer is composed of $M-2$ segments of length

$$m = r_f/(M-2)$$

and the current radius in this layer is

$$r_i = (i-1)m, \qquad i = 1,2,3,\ldots,M-2,M-1. \tag{28}$$

For an internal liquid layer and an external solid layer:

$$n = (r_k-r_f)/(N-M),$$
$$r_i = m(M-2)+n(i+1-M), \qquad i = M-1,M,\ldots,N-2,N-1 \tag{29}$$

and

$$k = (r_e-r_k)/(K-N),$$
$$r_i = m(M-2)+n(N-M)+k(i+1-N), \qquad i = N-1,N,\ldots,K-2,K-1. \tag{30}$$

Evidently in the case described in 4.2. $M = N = K$ and $m = n = k$ and in the case of (4.3) and (4.4) $N = K$ and $n = k$.

Equation (10) using (25) and (26) can be written as follows:

$$T_{i+1} + b_i T_i + c_i T_{i-1} + d_i = 0, \tag{31}$$

where the factors b_i, c_i, d_i are:

for $i = 2, 3, \ldots, M-3, M-2$,

$$\left.\begin{aligned} c_i &= \left(\frac{i-1.5}{i-0.5}\right)^2 \frac{\lambda_i + \lambda_{i-1}}{\lambda_i + \lambda_{i+1}}, \\ d_i &= \left(\frac{i-1}{i-0.5}\right)^2 \frac{2m^2 \rho_i c_{pi} T_i^-}{\Delta t(\lambda_i + \lambda_{i+1})}, \\ b_i &= -1 - c_i - d_i / T_i^-. \end{aligned}\right\} \tag{32}$$

for $i = M, M+1, \ldots, N-3, N-2$,

$$\left.\begin{aligned} c_i &= \left[\frac{m(M-2) + n(i-M+0.5)}{m(M-2) + n(i-M+1.5)}\right]^2 \frac{\lambda_i + \lambda_{i-1}}{\lambda_i + \lambda_{i+1}}, \\ d_i &= \left[\frac{m(M-2) + n(i-M+1)}{m(M-2) + n(i-M+1.5)}\right]^2 \frac{2n^2 \rho_i c_{pi} T_i^-}{\Delta t(\lambda_i + \lambda_{i+1})}, \\ b_i &= -1 - c_i - d_i / T_i^- \end{aligned}\right\} \tag{33}$$

for $i = N, N+1, \ldots, K-3, K-2$,

$$\left.\begin{aligned} c_i &= \left[\frac{m(M-2) + n(N-M) + k(i-M+0.5)}{m(M-2) + n(N-M) + k(i-M+1.5)}\right]^2 \frac{\lambda_i + \lambda_{i-1}}{\lambda_i + \lambda_{i+1}}, \\ d_i &= \left[\frac{m(M-2) + n(N-M) + k(i-M+1)}{m(M-2) + n(N-M) + k(i-M+1.5)}\right]^2 \frac{2k^2 \rho_i c_{pi} T_i^-}{\Delta t(\lambda_i + \lambda_{i+1})}, \\ b_i &= -1 - c_i - d_i / T_i^-. \end{aligned}\right\} \tag{34}$$

The value of the temperature at the points $i = 1$, $i = M-1$, $i = N-1$ and $i = K-1$ can be calculated from the boundary conditions.

The boundary condition (12) is expanded by the Taylor series and the first two terms after comparison the second derivatives are giving:

$$T_3 - 4T_2 + 3T_1 = 0. \tag{35}$$

The boundary condition for a stationary external diameter of the sphere (13) written in the finite difference form according to (27) is:

$$T_K - \left(1 + \frac{\lambda_{K-1}}{\alpha k}\right) T_{K-1} + \frac{\lambda_{K-1}}{\alpha k} T_{K-2} = 0$$

i.e. it has the same form as equation (31) with the following factors:

$$\left.\begin{aligned} c_{K-1} &= \frac{\lambda_{K-1}}{\alpha k}, \quad d_{K-1} = 0, \\ b_{K-1} &= -1 - c_{K-1} - d_{K-1} / T_{K-1}^-. \end{aligned}\right\} \tag{36}$$

Similarly equations (14) and (19) can be formulated as (31) with the factors:

$$\left.\begin{aligned} c_i &= \frac{\lambda_i + \lambda_{i-1}}{\lambda_i + \lambda_{i+1}} \frac{r_{i+1} - r_i}{r_i - r_{i-1}}, \\ d_i &= \frac{2L_f \rho_i \Delta r(r_{i+1} - r_i)}{\Delta t(\lambda_i + \lambda_{i+1})}, \\ b_i &= -1 - c_i, \end{aligned}\right\} \tag{37}$$

where $i = M-1$ for equation (14) and $i = N-1$ for equation (19) and r are the changes of melting or solidification radii.

When the function describing the thermal conductivity of the sphere material is continuous at the melting temperature, this equation can be simplified by replacing $(\lambda_i + \lambda_{i-1})/2$ and $(\lambda_i + \lambda_{i+1})/2$ by λ_i.

In the case of evaporation at the outer boundary, condition (16) is relevant instead of (13). In difference form this can be expressed by equation (31) with the factors:

$$\left.\begin{aligned} &\text{for } i = K-1, N = K \text{ and } n = k, \\ c_{K-1} &= \frac{\lambda_{K-1}}{\alpha k}, \quad b_{K-1} = -1 - c_{K-1}, \\ d_{K-1} &= \frac{L_e \rho_{K-1}}{\alpha \Delta t} \Delta r_e, \end{aligned}\right\} \tag{38}$$

where Δr_e is the variation of the evaporation radius. The temperature at the point K is the gas temperature:

$$T_K = T_g. \tag{39}$$

Then we obtain the following set of equations:

$$\left.\begin{aligned} &T_3 - 4T_2 + 3T_1 = 0, \\ &T_{i+1} + b_i T_i + c_i T_{i-1} + d_i = 0, \\ &\quad (i = 2, 3, \ldots, K-2, K-1), \\ &T_K = T_g, \end{aligned}\right\} \tag{40}$$

with factors described as follows:

for the one-phase case by (32) and (36), for the two-phase case by (32), (33), (36) and (37), for the

case of evaporation by (32), (33), (37) and (38), for the case of solidification by (32)–(34), (36), (37).

In the case of diffusion of the particle material the same set of equation is used, but the value of evaporated radius can be calculated directly from (24).

The above set of equations can be easily solved by the method of the factorization first forward and then backwards [16].

Looking for a solution in the form:

$$\left.\begin{aligned} &T_i = h_{i+1} + g_{i+1} T_{i+1} \\ &\text{for } i = K-1, K-2, \ldots, 3, 2 \end{aligned}\right\} \tag{41}$$

the required factors are:

$$\left.\begin{aligned} &g_{i+1} = -1/(b_i + c_i g_i), \\ &h_{i+1} = (d_i + c_i h_i) g_{i+1}, \\ &\text{for } i = 2, 3, \ldots, K-2, K-1. \end{aligned}\right\} \tag{42}$$

These factors depend on the coefficients of equation (31) and it is possible to calculate the values of temperature (41) from the values of g_1 and h_1 [known from (12)].

The convergence and accuracy of the used scheme is $O(h^2+\tau)$ [16], where the reduced time $\tau = 4\lambda\Delta t/\rho c_p D^2$ and the reduced co-ordinate $h = 2\Delta r/D$.

Values of the phase change radii Δr_f, Δr_k and Δr_e [in equations (37) and (38)] must be arbitrarily assumed in the first approximation and they will result from the iteration process. Equations (15), (17) and (20) will be used for checking the accuracy of the results obtained [equation (17) only in case of intense evaporation].

The values of material parameters, on which the factors of equation (31) depend, should be taken for the actual calculated values of the temperature at the given point. For more accurate calculations an iterative method was used to obtain the relevant coefficients.

In Fig. 2 the flow chart of the computer program is given. This program was made in FORTRAN IV Extended for the computer CDC-6000 Cyber 70.

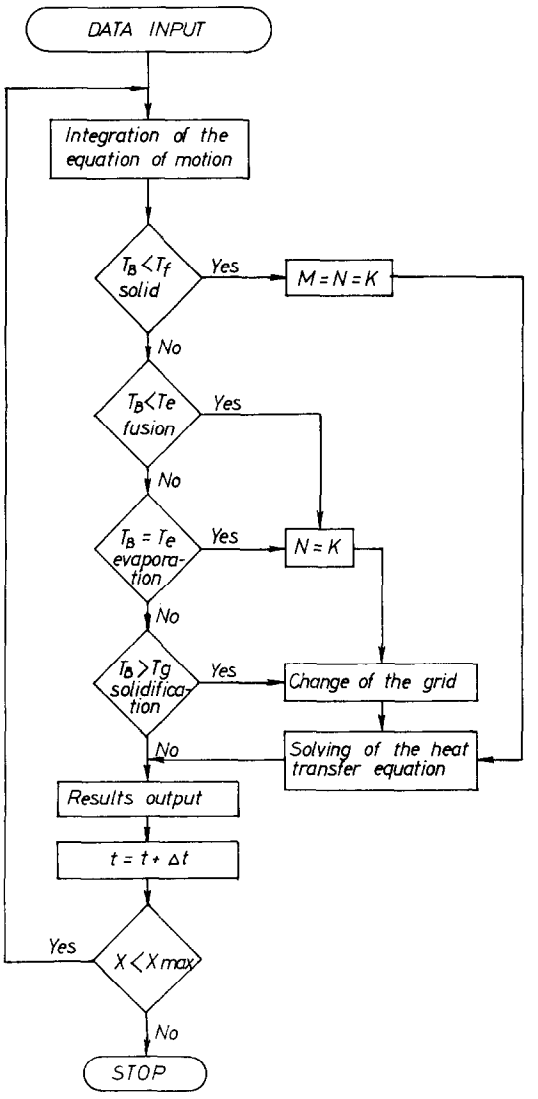

FIG. 2. Flow chart of computer program.

6. RESULTS OF CALCULATIONS

A series of calculations for alumina grains with an initial diameter up to 120 μm and velocities of injection up to 30 m/s were made. The results of calculations made for an Al_2O_3 particle with a diameter 100 μm and an initial velocity 10 m/s are shown on Fig. 3. Five zones are visible:

I—heating to the melting temperature on the surface;

II—heating to the evaporation temperature on the surface with simultaneous melting of the particle interior and evaporation by diffusion of mass at the surface;

III—intensive evaporation from the surface with a temperature equal to T_e;

IV—cooling down to obtain the solidification temperature at the surface;

V—solidification of the particle.

In the first two regions the increase of the particle temperature is very fast because of a high gas and surface temperature difference. In the third region, during the evaporation, the change of the external diameter is very fast and the temperature differences inside the particle disappear. The fourth region begins when the particle leaves the high temperature region of the jet. The temperature drops at the surface faster than at the centre. When the surface temperature reaches the solidification temperature (region V), the process of solidification begins. The profiles of the temperature inside this particle at the end of region I (curve 1), region II (curve 2), and in region V (curve 3) are shown at the Fig. 4. They appear to be parabolic.

Results of calculations for alumina particles injected with initial velocities from 3 to 30 m/s are shown on Fig. 5. The influence of the particle initial velocity can be seen. Particles with too low an injection velocity do not enter into the high

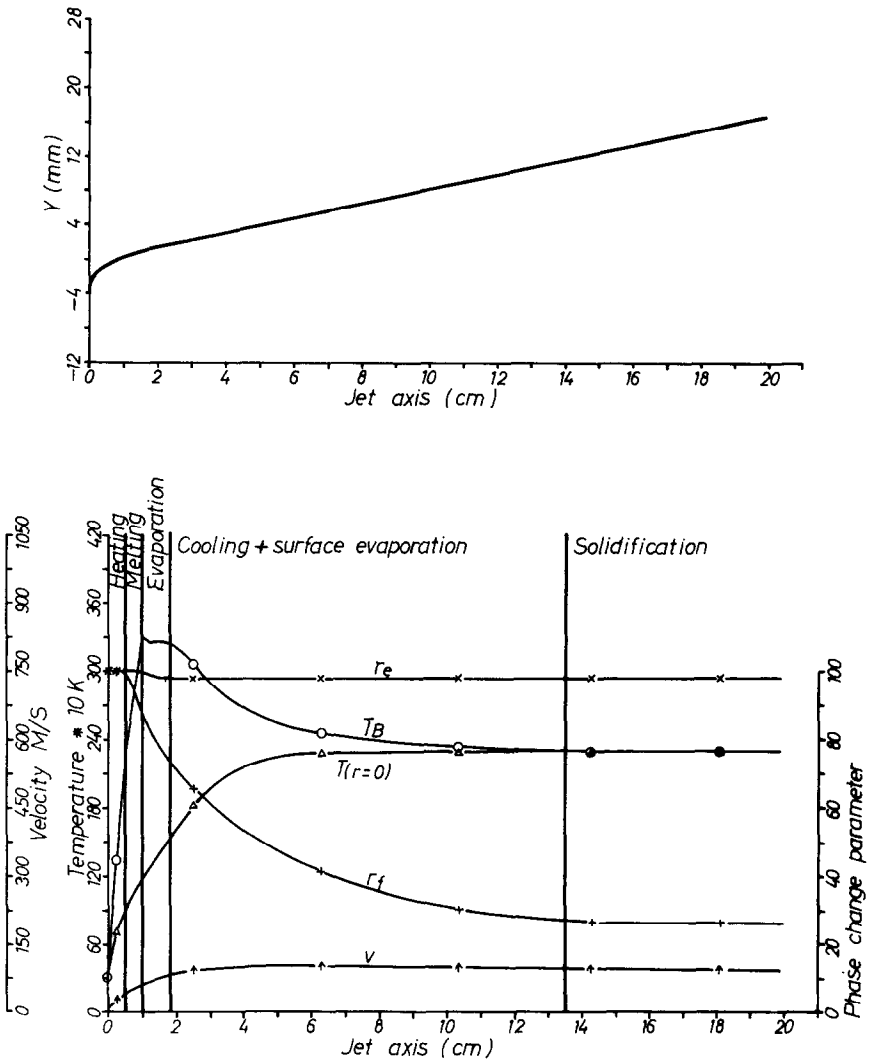

FIG. 3. The melting process of an alumina particle 100 μm dia injected with a velocity 10 m/s.

temperature region of the jet and are not melted. With too large an injection velocity the dwell time in the high temperature region of the jet is too small for melting to occur. There are some values of injection velocity for which the particle evaporation rate is too large. This can be seen on Fig. 5a where the trajectories of particles are presented together with curves indicating when the melting or evaporation temperature are achieved. The lines are also shown where the particle is melted up to one half of its radius, the particle is completely melted and constant evaporation rate lines (at which the sphere radius is reduced by 10%, 20%, 30%) are presented. Maximum evaporation of 36% was obtained for the particle injected with a velocity of 13 m/s. This is visible on Fig. 5b. The influence of the initial velocity on the particle velocity (Fig.. 5c) and temperature (Fig. 5d) are also shown.

To demonstrate the influence of the diameter changes on the trajectory, some calculations were made for the particles with a fixed diameter (and mass). Comparison of the obtained trajectories (Fig. 6) shows that these differences do not exceed 10%.

Using the results of the numerical calculations for Al_2O_3 grains with different initial diameters, the regions where the grains with a given diameter (initial) are completely melted (Fig. 7) can be shown. These regions are below the jet axis on the side opposite to the point of injection. This is associated with the method of powder injection. It was found that Al_2O_3 particles of a diameter 120 μm are not completely melted in any region of the jet and the particles of a diameter 30 μm or less are completely evaporated in some regions.

The influence of non-perpendicular injection of powder was examined (Fig. 8). The influence of the angle of injection (in the plane formed by the point of injection and the jet axis) $-\varphi-$ is very small and does not exceed 4% for Al_2O_3 particles of 50 μm diameter injected with a velocity of 10 m/s at an angle $\varphi = 15°$. The influence of eccentric injection is much higher. The same size grain in the plane

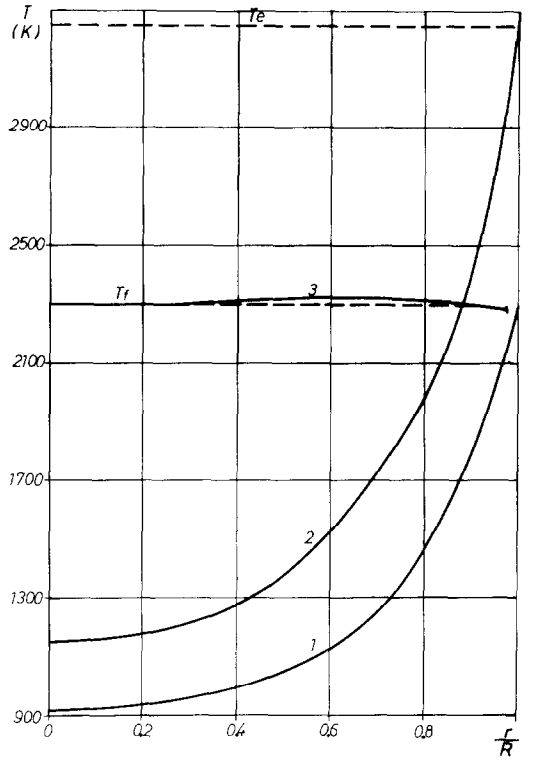

FIG. 4. Temperature profiles of an Al_2O_3 100 μm dia particle injected perpendicularly to the jet axis with a velocity of 10 m/s.

passing at a distance $b = 2$ mm from the jet axis has an external diameter 17% greater and velocity 13% smaller than the grain crossing the jet axis.

7. COMPARISON OF THE CALCULATED AND EXPERIMENTAL RESULTS*

Experimental results refer to Al_2O_3 powder with an average diameter 47 μm (the diameters of the particles were between 30 μm and 67 μm) while the calculations were made for particles with a few selected diameters. For the comparison of the available results the powder was divided into three fractions: 35–45 μm, 45–55 μm and 55–65 μm and it was assumed that the particles enclosed in these fractions have diameters of 40, 50, and 60 μm respectively. With the known experimental injection velocities of particles (Fig. 9) and their granulometric distribution at the inlet to the jet (curve 1, Fig. 10) it was possible to calculate the distributions at the jet exit (curve 3, Fig. 10) and to compare it with the experimental curve (2, Fig. 10). The calculated curve is about 25% wider and its maximum is displaced by about 20% into the direction of lower diameters than the experimental curve. This difference may be due to neglecting in the calculations the actual scatter of particle trajectories with respect to the jet axis. The numerical calculations are strictly correct only for particles whose trajectories pass through the jet axis.

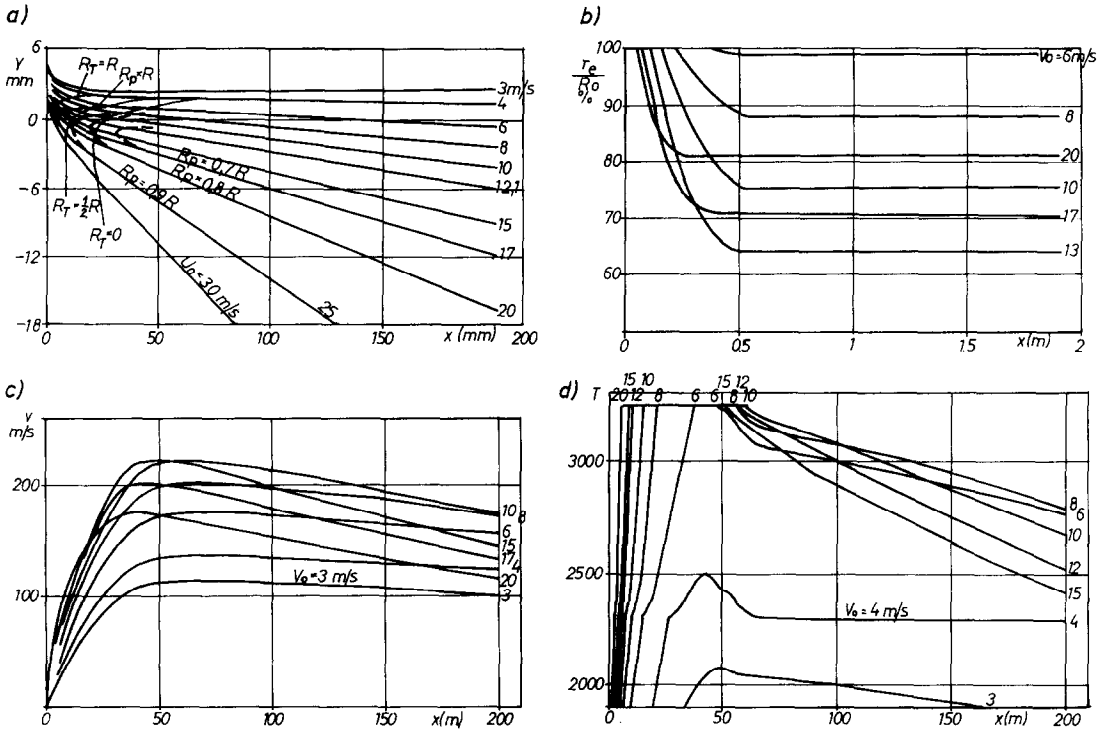

FIG. 5. Variation of trajectories (a), diameters (b), velocities (c) and surface temperatures (d) of Al_2O_3 50 μm dia particles, injected perpendicularly with different velocities, versus the distance from the jet origin.

*All experimental results were taken from J. Lesinski measurements—Ph.D. Thesis made in the Institute of Nuclear Research, 05-400, Otwock, Poland, 1975.

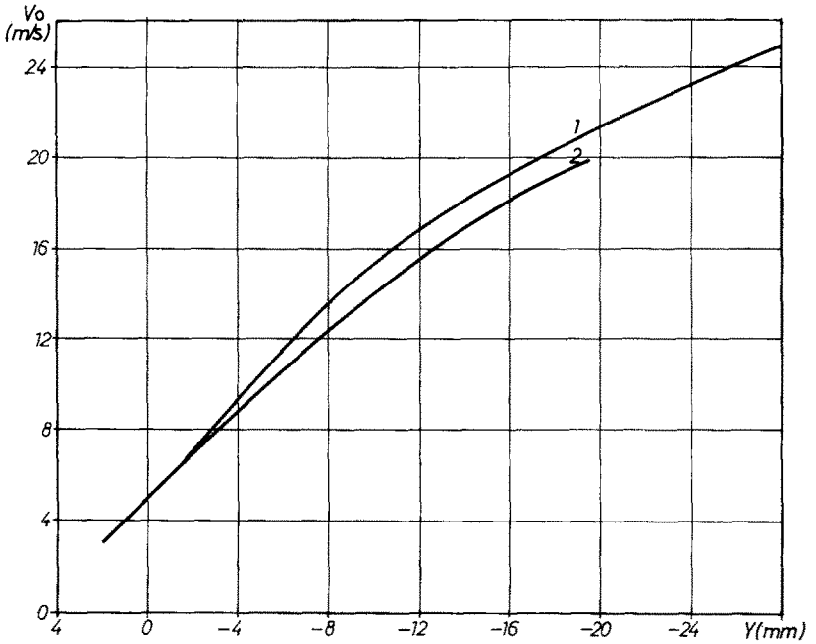

FIG. 6. Dependence of the position of the particle in the jet cross-section, distant 200 mm from the jet origin, on the injection velocity of Al_2O_3 particles of initial diameter 50 μm. Curve 1—taking into account the variation of the diameter, curve 2—for constant diameter particles.

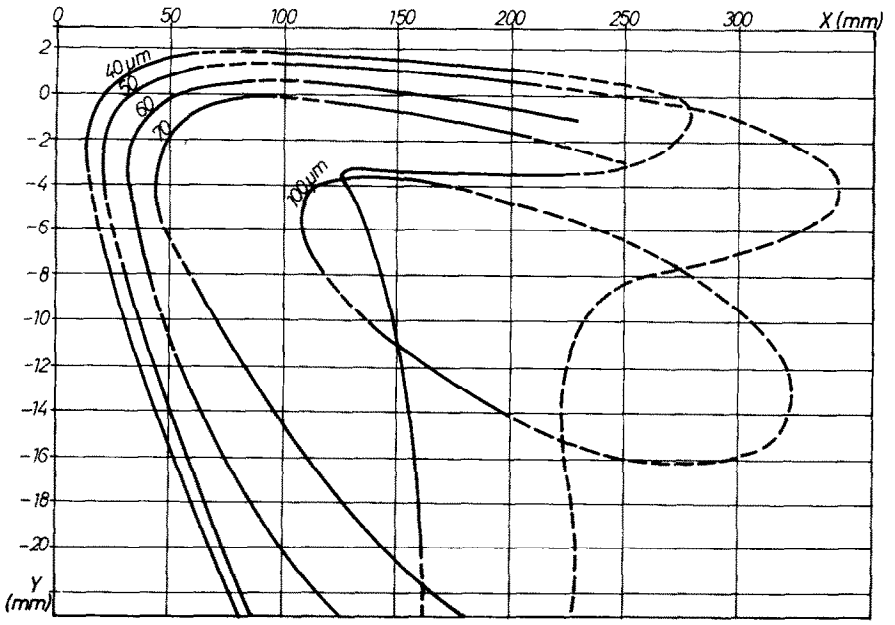

FIG. 7. Regions of complete melting of alumina particles injected perpendicularly into the plasma jet.

The observed 20% difference between the positions of the maxima of the calculated and measured velocity distribution (Fig. 11) may be due to the same reason as above. As shown in Section 6 (Fig. 8) particles eccentrically injected have velocities and diameter changes much lower than those passing through the jet axis. The variation of the particles' average temperature with distance from the jet exit is shown on Fig. 12. The difference between the calculated (continuous line) and measured (circles with range of accuracy indicated by bars) average particle temperature is only about 15%.

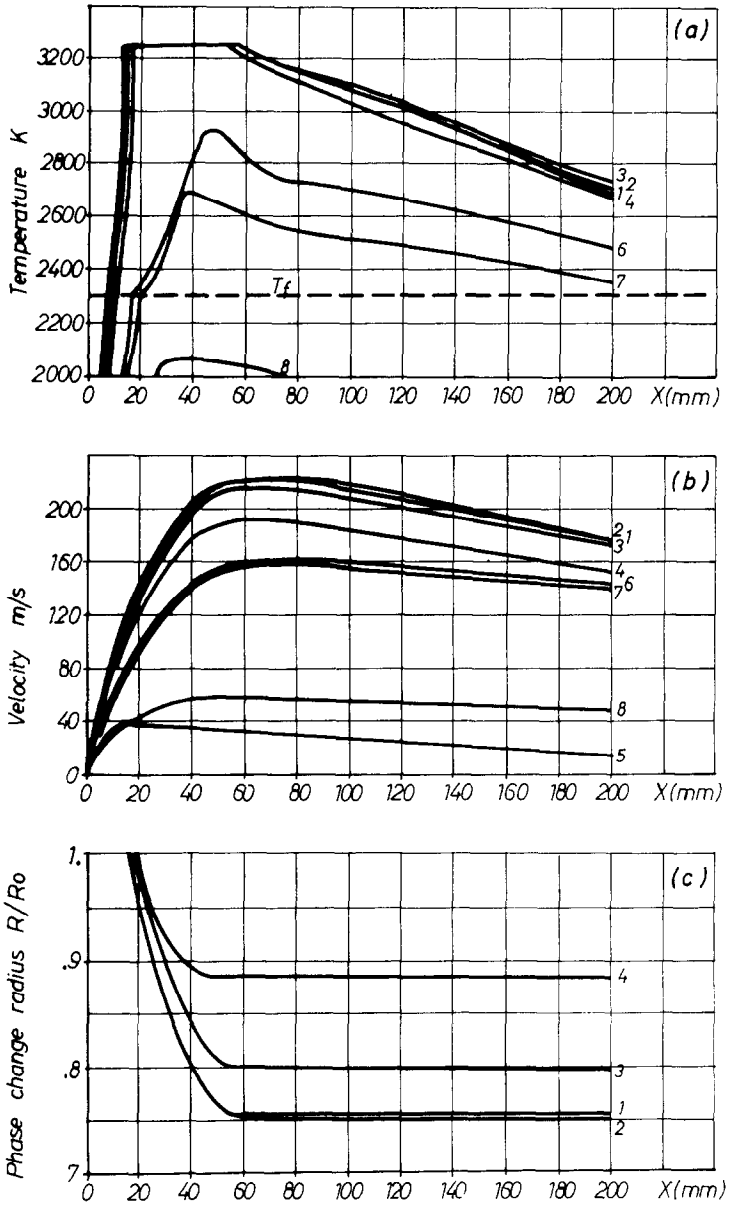

FIG. 8. Variation of some parameters of Al_2O_3 50 μm dia particles, injected non-perpendicularly into the plasma jet vs distance from jet origin ($v_0/\varphi/b$). Curve 1—(10/0/0), 2—(10/−15/0), 3—(10/+15/0), 4—(10/0/2), 5—(10/0/3), 6—(5/0/0), 7—(5/0/2), 8—(5/0/3).

From the above it can be concluded that the qualitative agreement between the principal measured and calculated parameters is satisfactory and the divergences can be explained by the influence of the following factors:

—calculations were made for particles of selected diameters, with trajectories in the plane passing through the jet axis (i.e. through the region with maximum thermophysical jet parameters) while in practice powder is introduced into the jet as a divergent cluster having a certain width and a disperse granulation,

—the thermophysical properties of plasma gases and particle material were taken from published data, which differ appreciably, or in cases when these data were not available they were calculated using approximate formulae,

—there exists a small temperature difference between the evaporating particle surface and the evaporation temperature of the particle medium, this difference was neglected as this value was unknown,

—the measured powder velocities were obtained from a small number of measurements and exhibited a large velocity scatter,

—the measurements of the powder temperature were based onto rough assumptions. In particular the material emissivity (at the temperature higher than

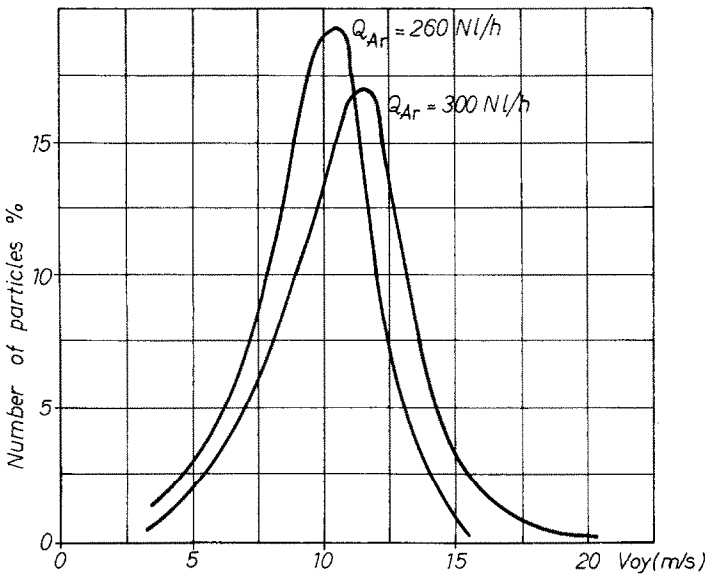

FIG. 9. Velocity distribution of Al_2O_3 particles at the inlet to the plasma jet (for two rates of flow of the particles carrying gas).

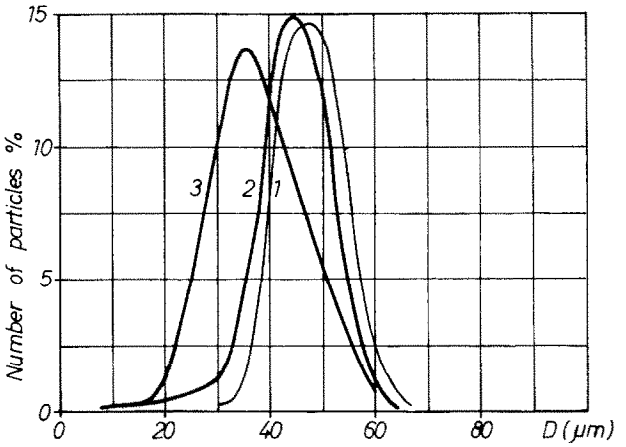

FIG. 10. Distribution of the diameters of particles used in experiments: 1—at the inlet into the jet, 2—at the jet outlet (measured), 3—at the jet outlet (calculated).

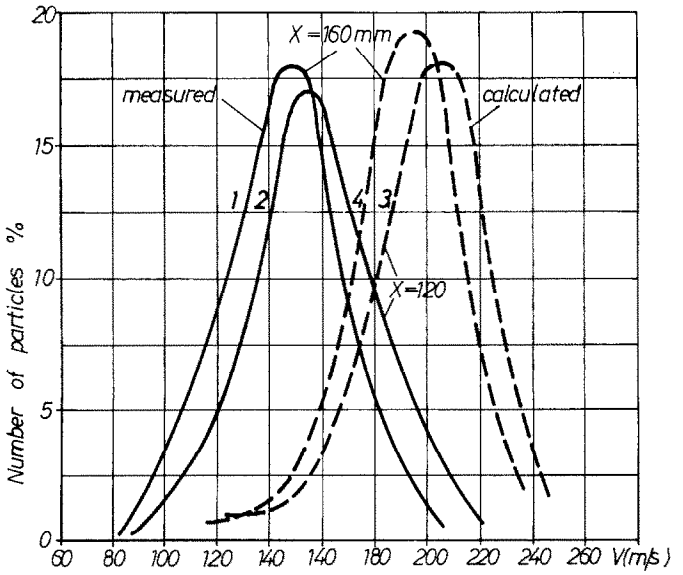

FIG. 11. Velocity distribution of the Al_2O_3 particles in the plasma jet.

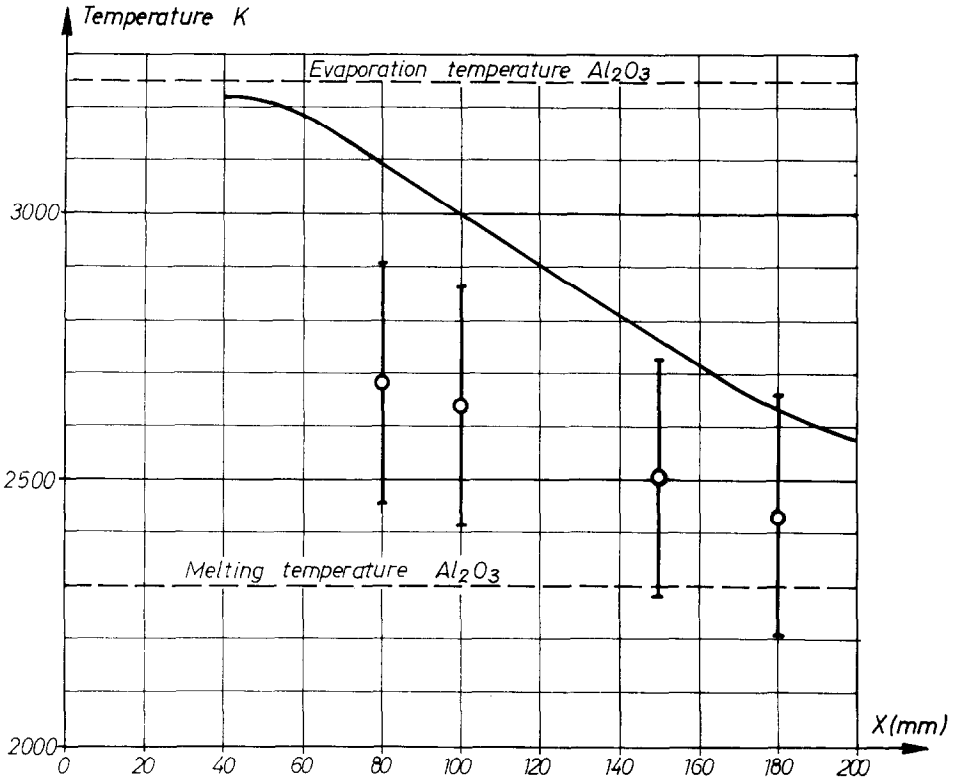

FIG. 12. Variation of the average temperature of the particles with the distance from the jet origin.

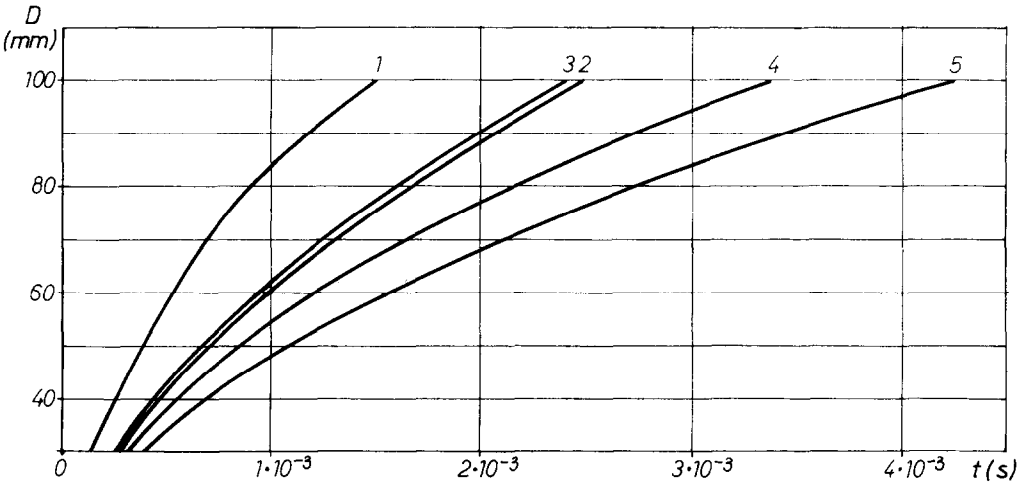

FIG. 13. Comparison of the time necessary to melt a spherical particle obtained in present model and in model of Dresvin [17].

temperature of fusion) was unknown and the important influence of particle diameter scatter on the deduced temperature was not taken into account.

The results of numerical calculations were compared with the known approximate formula [17] giving the time necessary for complete melting of spherical particle. This formula is based on the assumption of uniform temperature inside the particle, constant temperature and velocity of the medium and that the particle is stationary with respect to the gas medium. Figure 13 shows the calculation using [17] (curves 4 and 5) melting times for Al_2O_3 and W as a function of particle diameter. These times were calculated for an Ar–H_2 plasma temperature of 8000 K, Curves 2 and 3 were obtained from numerical calculations using the method given in this paper for constant gas temperature and velocity ($T_g = 8000$ K, $V_g = 540$ m/s). Curve 1 shows the minimum necessary time for melting Al_2O_3 grains under actual conditions according to the present calculations. A large

difference between these calculations, especially for particles with greater diameters, is observed. From this figure it appears that approximate formulae such as the one given by (17) do not take into account the main factors which influence the investigated process.

8. CONCLUSIONS

The method of calculation used in this paper for heating processes including phase changes, for spherical particles moving in a hot gas stream, allows for the change of jet parameters and the variation with temperature of the physical properties of the gas medium and of the particle.

It should be noted that the numerical method presented above does not include the influence of real particle injection conditions which are stochastic in the velocity vector and particle size distributions. It would be useful to develop this method to include such effects.

REFERENCES

1. H. S. Carslaw and J. C. Jaeger, *Conduction of Heat in Solids*, p. 276. Clarendon Press, Oxford (1959).
2. A. V. Luikov, *Teoria Teploprovodnosti (Theory of Heat Conduction)*, p. 436. Moscow (1967).
3. M. I. Dubovis, *Issledovania po Teploprovodnosti (Investigations in Heat Conductivity)*, p. 326. Minsk (1967).
4. R. I. Pedroso and G. A. Domoto, Inward spherical solidification—solution by the method of strained coordinates, *Int. J. Heat Mass Transfer* **16**, 1816–1824 (1973).
5. N. Frösling, Uber die Verdunstung Fallender Tropfen, *Gerl. Beit. Geophys.* **52**, 170 (1938).
6. G. D. Raithby and E. R. Eckert, The effect of turbulence parameters and support position on the heat transfer from spheres, *Int. J. Heat Mass Transfer* **11**, 1233–1238 (1968).
7. W. S. Klubnikin, *Voprosy Fizyki Nizkotemperaturnoi Plazmy (Problems in Low Temperature Plasma Physics)*, p. 43. Minsk (1970).
8. J. Fay and F. R. Riddl, Theory of stagnation point heat transfer in dissociated air, *J. Aeronaut. Sci.* **25**, 73–85 (1958).
9. G. L. Babucha and M. I. M. Rabinovitsh, *Mechanika i Teploobmen Potokov Polidispersnoi Gazovzvesi (Mechanics and Heat Transfer in Polidispersed Streams)*. Kiev (1969).
10. R. B. Bird, W. E. Stewart and E. N. Lightfoot, *Transport Phenomena* (Russ. Transl.), p. 384. Moscow (1974).
11. I. Kimura and A. Kanzawa, Experiments on heat transfer to wires in a partially ionized argon plasma, *AIAA Jl* **3**, 476–481 (1965).
12. E. V. Seymour, The hydrodynamic drag on a small sphere in an ionized gas, *Trans. ASME—J. Appl. Mech.* 739–748 (Dec. 1971).
13. R. E. Treybal, *Mass Transfer Operations*. McGraw-Hill, New York (1955).
14. N. S. Surov, Eksperimentalnoie issledovanie raspredelenia parametrov v odnofaznych i dvuchfaznych plazmennych strujach (Experimental investigation of the distribution of parameters in one- and two-phase subsonic plasma jet), *Teplofiz. Vysok. Temp.* **7**, 305–312 (1969).
15. K. A. Zischka and P. S. Chow, On non-linear initial boundary value problems of heat conduction and diffusion, *SIAM Rev.* **16**, p. 17 (1974).
16. A. A. Samarskij, *Vvedenie v Teoriu Raznostnych Schem (Introduction to the Theory of Differential Methods)*, p. 275. Moscow (1971).
17. V. S. Dresvin, *Fizika i Technika Nizkotemperaturnoi Plazmy (Physics and Technology of Low Temperature Plasma)*, p. 342. Moscow (1972).

FUSION DES GRAINS SPHERIQUES DANS UN JET DE PLASMA

Résumé—Une méthode numerique pour la détermination de l'échange du chaleur et de la variation de phase entre une sphère solide et le plasma est deduit. Le variation des propriétés thermophysiques de particule solide et de plasma avec la temperature sons inclus. Un example des particules de Al_2O_3 chauffées dans un jet de plasma d'argon–hydrogene est donne. La comparaison des résultats numeriques avec les résultats expérimentaux concernant la température de la surface, de la velocité et du diamètre de particule est satisfaisant.

SCHMELZEN VON PULVER-KÖRNERN IN EINER PLASMA-FLAMME

Zusammenfassung—Zur Berechnung des Wärmeübergangs und des Phasenwechselvorganges eines kugelförmigen Teilchens in einer Strahlströmung wird eine numerische Berechnungsmethode aufgestellt. Dabei wird die Temperaturabhängigkeit der thermophysikalischen Eigenschaften des Teilchens und des Plasmas in Betracht gezogen. Als Beispiel werden Aluminiumteilchen betrachtet, die in einem Argon–Wasserstoff–Plasmastrahl aufgeheizt werden. Die numerischen Ergebnisse zeigen gute Übereinstimmung mit experimentell gemessenen Werten der Oberflächentemperaturen des Teilchendurchmessers und der Teilchengeschwindigkeit.

ПЛАВЛЕНИЕ ЗЁРЕН ПОРОШКА В ПЛАЗМЕННОМ ФАКЕЛЕ

Аннотация — Разработан численный метод исследования процессов теплообмена и фазовых изменений сферической частицы в струйном потоке. Учитывается температурная зависимость теплофизических характеристик частицы и плазмы. Рассмотрен пример нагрева алюминиевых частиц в струе аргоно-водородной плазмы. Получено хорошее совпадение численных результатов с данными измерений температуры поверхности, скорости и диаметра частиц.